Supporting Information for

Synthesis and magnetic properties of sub-nanosized iron carbides on a carbon support

Masanori Wakizaka[1], Wang-Jae Chun[2], Takane Imaoka[1,*], and Kimihisa Yamamoto[1,*]

[1]Laboratory for Chemistry and Life Science Institute of Innovative Research, Tokyo Institute of Technology, Yokohama 226-8503, Japan.

[2]Graduate School of Arts and Sciences, International Christian University, Tokyo 181-8585, Japan.

Contents

Methods

Materials. TPM-DPAG4 was prepared according to previously reported procedures.[33–36] $FeCl_3$, α-Fe_2O_3, Fe_3O_4, boron nitride (BN), and graphitized mesoporous carbon (GMC) were purchased from Sigma-Aldrich. Dehydrated acetonitrile (MeCN), dehydrated chloroform ($CHCl_3$), dehydrated *n*-hexane, and methanol (MeOH) were purchased from Kanto Chemical Co. Aqueous HCl and HNO_3 were purchased from Fujifilm Wako Pure Chemical Corp. The GMC was washed with distilled water and MeOH, followed by filtration and drying *in vacuo*. The GMC was subsequently heated for 3 h to 1173 K under a H_2 (99.99999%) flow (200 mL min^{-1}). Bulk Fe_3C was prepared as a gray powder from the CO reduction of Fe_3O_4 according to a reported procedure (Fig. S5).[10]

Titration. 3000 μL of MeCN/$CHCl_3$ (1:1, *v*/*v*) solutions of TPM-DPAG4 (3.0 μM) were prepared in an optical quartz cell (optical path = 1.0 cm) under a dry N_2 atmosphere (ca. 1 ppm water and oxygen) at room temperature. Defined amounts (1 eq. × 4 times, 2 eq. × 4 times, 4 eq. × 4 times, and 8 eq. × 4 times; 60 eq. total) of the MeCN solutions of $FeCl_3$ (3.0 mM) were then continually added to the solution using a micropipette. The complexation behavior was monitored at each titration step using UV-Vis spectroscopy.

Preparation of the precursor samples for Fe_4/C, Fe_{12}/C, Fe_{28}/C, and Fe_{60}/C. Pale yellow solutions of TPM-DPAG4 (3.00 μM) in 180 mL of MeCN/CH_2Cl_3 (1:1, *v*/*v*) were prepared under a dry Ar atmosphere at room temperature. A MeCN solution of $FeCl_3$ (4, 12, 28, or 60 eq.) was then added to the TPM-DPAG4 solution. After stirring for 45 min, the solutions turned deep yellow. The stirred solutions were added dropwise to the individually stirred suspensions of GMC (180 mg) in $CHCl_3$ (30 mL) dispersed under sonication (30 W) for 3 min. After filtration, the resultant powder samples

(precursors for **Fe_4/C**, **Fe_{12}/C**, **Fe_{28}/C**, and **Fe_{60}/C**) were washed with *n*-hexane (2 × 5 mL) and dried *in vacuo* for 2 h. In addition, another batch sample for **Fe_4/C** was synthesized as sample B by the same procedure.

Carbothermal hydrogen reduction (CHR). The precursor samples for **Fe_4/C**, **Fe_{12}/C**, **Fe_{28}/C**, and **Fe_{60}/C** were heated in a quartz boat at 773 K for 30 min under a flow of H_2 (99.99999%, 100 mL min^{-1}) in a furnace at a heating rate of 24 K min^{-1}. The samples were handled under an Ar atmosphere, both before and after the reduction.

Measurements. PXRD measurements were conducted at room temperature using Cu Kα radiation on a Rigaku Ultima IV diffractometer. UV–vis spectra were recorded at 293 K under the ambient atmosphere using a Shimadzu UV-2700 spectrophotometer. Inductively-coupled plasma atomic emission spectroscopy (ICP-AES) was conducted at Suzukakedai Materials Analysis Division (Tokyo Tech.). The analytes were extracted using an aqueous acid solution (HCl 23% and HNO_3 20%) under sonication (35 W) for 6 min, and the resulting solutions were diluted five-fold for analysis. TEM (JEOL JEM-ARM200F ACCELARM) images were recorded with an accelerating voltage of 80 kV. The analytes were dispersed in *n*-hexane, dropped onto micro-Cu grids with carbon filaments (thin holey carbon film coated grids, Alliance Biosystems), and dried for >12 h *in vacuo* at room temperature. XAFS spectra were measured in transmission and fluorescence modes at room temperature at the BL-9C beamline (Photo Factory, High Energy Accelerator Research Organization (KEK-PF), Tsukuba, Japan; ring energy: 2.5 GeV). Incident X-ray beams were monochromated by channel-cut monochromators using Si(111), detuned to 60%. Detectors used two ionization chambers (one filled with N_2 for I_0 and one filled with N_2/Ar (75:25) for I) in transmission mode, and a Lytle

detector filled with Ar in fluorescence mode. The **Fe_{60}/C** sample after CHR was packed in a vinyl chloride tube (7 mm diameter) and wrapped in a gas barrier film (silica deposited nylon/polyethylene) under an Ar atmosphere for measurements in transmission mode. The **Fe_4/C**, **Fe_{12}/C**, and **Fe_{28}/C** samples after CHR were pelletized (7 mm diameter) and wrapped in a Kapton polyimide film under an Ar atmosphere for measurements using fluorescence mode. Fe_3C, $FeCl_3$, α-Fe_2O_3 and Fe_3O_4 were pelletized (10 mm diameter) by mixing with BN for measurements in transmission mode. The absorption energies of all samples were corrected using that of an Fe foil as a reference. XAFS analyses were performed using Athena in the software package Demeter 0.9.26.

Magnetic measurements. Magnetic measurements were performed using a magnetic property measurement system (MPMS-7 or -XL, Quantum Design) with/without an oven in direct current mode. The sample (ca. 20 mg for the iron carbide clusters and a GMC blank) was filled into a gelatin capsule (0.13 mL, Matuya) which was fixed in a plastic straw for measurements below room temperature. For measurements above room temperature, the sample was fixed in a quartz tube (3 mm diameter) using quartz wool that was connected to the rod using copper wire (0.2 mm). The *M*–*H* loop was measured at 300 K and 1.9 K over the range of –4 to 4 T at intervals of 500 Oe (–1 to 1 T) or 5000 Oe (outside this range), using a standard transport for Fe_3C, **Fe_{60}/C**, **Fe_{28}/C** and **Fe_{12}/C** or a reciprocating sample option (RSO) transport for **Fe_4/C**. The magnetization data were measured three times at the applied field after stabilization and were averaged excluding outliers. The diamagnetic component of the magnetization, which was measured using pure GMC, was subtracted from the magnetization data. The *M*–*T* curves were measured between 300–600 K in increments of 5 K (near T_C and T_B) or 10 K (other range) at 5000 Oe for the Curie point measurement, or 500 Oe for the FC and ZFC measurements. For the FC and ZFC measurements, the sample was preheated to 520

K for 10 min with/without a field (500 Oe). The magnetization data were measured three times at the applied temperature after stabilization and averaged excluding outliers.

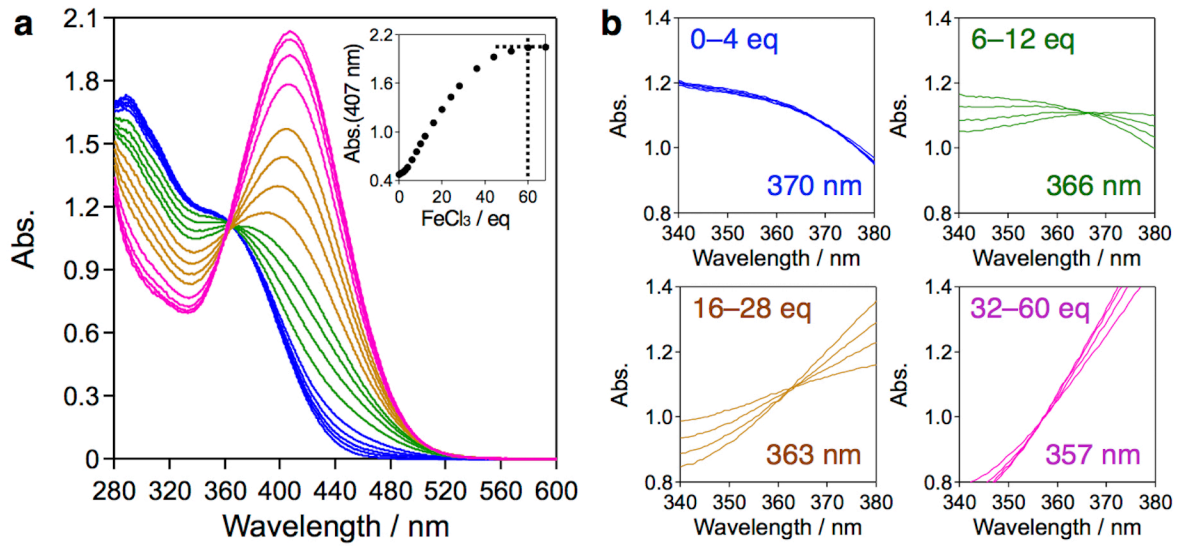

Fig. S1 (**a**) Changes in the full-scale UV–vis spectrum of TPM-DPAG4 (3.0 μM, in MeCN/$CHCl_3$ = 1/1, *v*/*v*) upon addition of 0–4 (blue lines), 6–12 (green lines), 16–28 (brown lines), and 32–60 (magenta lines) eq. of $FeCl_3$ in MeCN. Inset: plot of the absorbance at 407 nm for 0–68 eq. (**b**) Magnification of the isosbestic points.

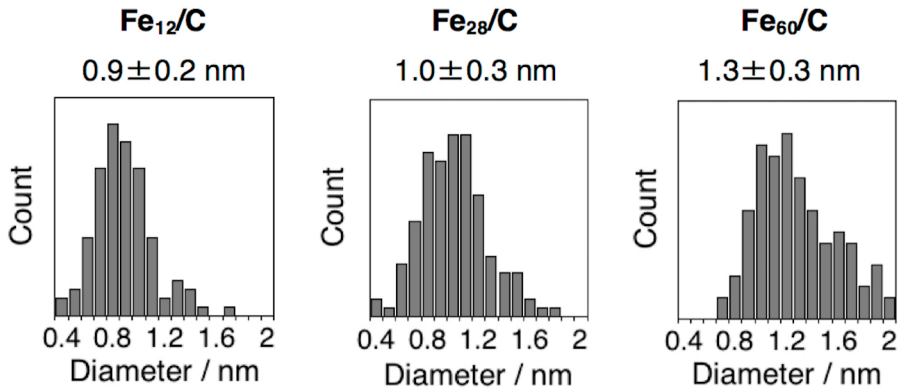

Fig. S2 Histograms of the particle-size distribution obtained from TEM images of **Fe_{12}/C**, **Fe_{28}/C**, and **Fe_{60}/C** after 30 min of CHR at 773 K.

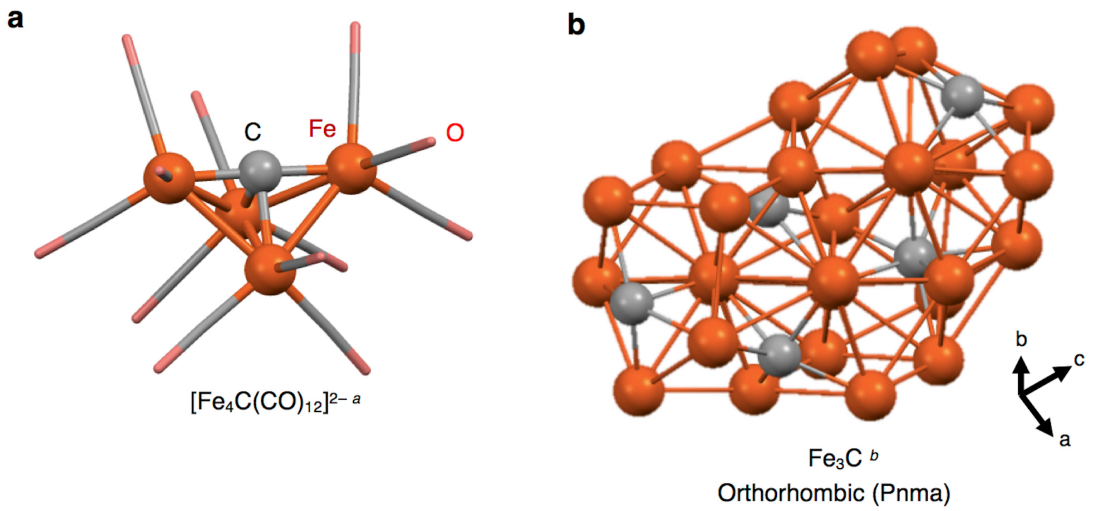

Fig. S3 The structure of (a) $[Fe_4C(CO)_{12}]^{2-}$ and (b) Fe_3C with a ball-and-stick model. [a] ref 40. [b] refs 43, 44.

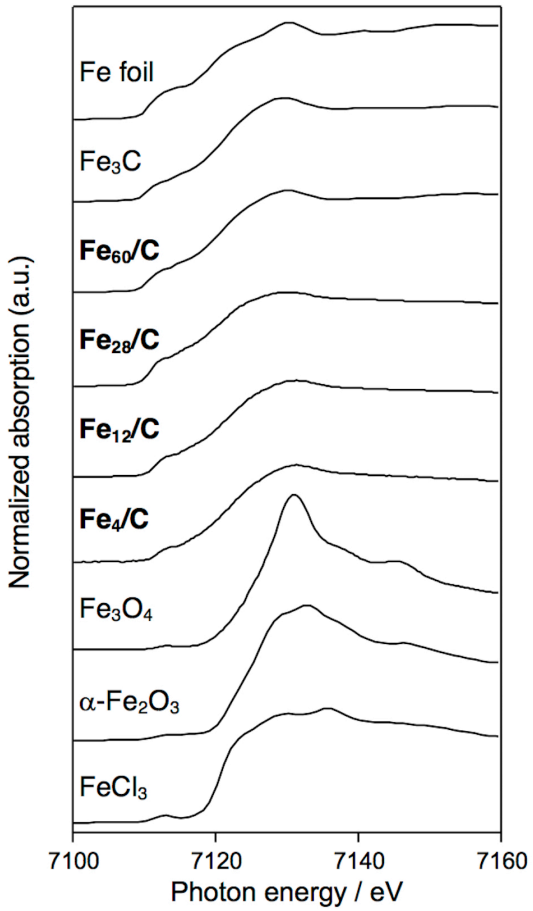

Fig. S4 Normalized Fe K-edge XANES spectra of **Fe_{60}/C**, **Fe_{28}/C**, **Fe_{12}/C**, and **Fe_4/C** after CHR at 773 K for 30 min, together with those of Fe foil, Fe_3C, Fe_3O_4, and α-Fe_2O_3. The spectra of **Fe_{28}/C**, **Fe_{12}/C**, and **Fe_4/C** were recorded in fluorescence mode, whereas others were recorded in transmission mode.

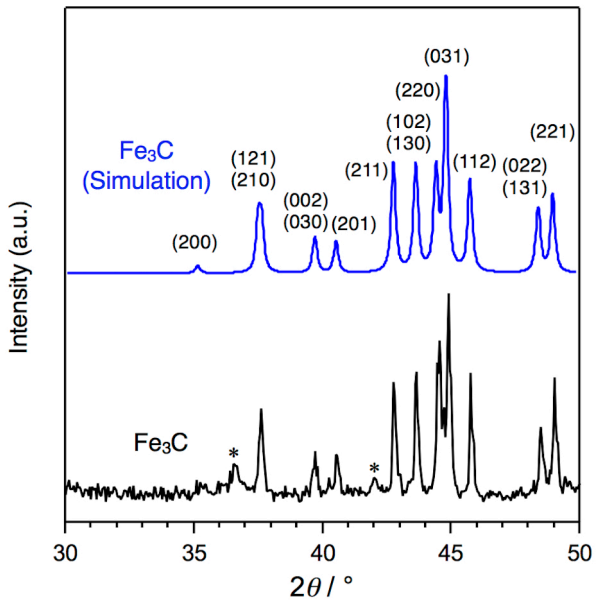

Fig. S5 PXRD patterns of Fe_3C (black line) together with that of the simulated pattern (blue line) where the applied the peak width at half the maximum intensity (FWHM) is $2\theta = 0.21°$.[43,44] *These peaks show the diffraction derived from impurities such as FeO.

The crystal size (D) was estimated by Scherrer's equation (Eq. S1), wherein K, λ, and β refer to the dimensionless shape factor = 0.9, the wavelength of X-ray, and the FWHM, respectively.

$$D = \frac{K\lambda}{\beta \cos\theta} \qquad \text{(Eq. S1)}$$

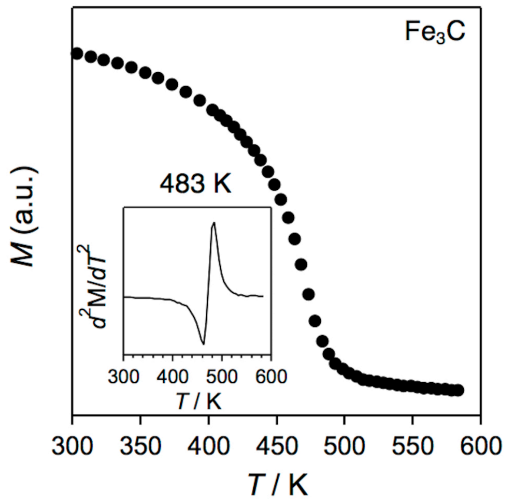

Fig. S6 The temperature-dependent magnetization curve for Fe_3C obtained by application of a magnetic field (5000 Oe) and measurement of the magnetization in increments of 10 K (300–420 K) or 5 K (420–600 K). The Curie point (T_C) was determined from the maximum of the second derivative (insets) and calibrated using T_C = 483 K for Fe_3C.[9]

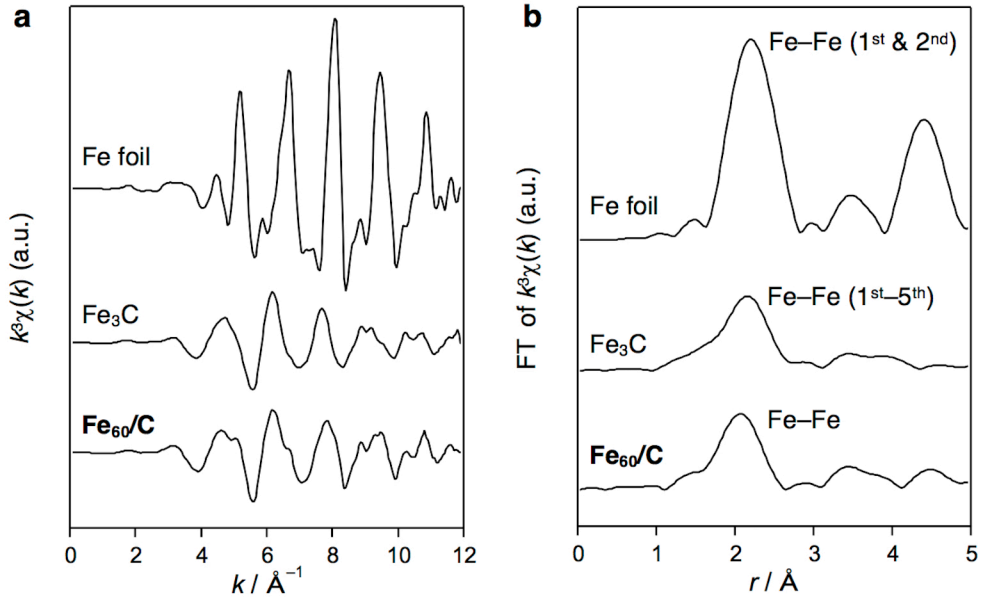

Fig. S7 Fe K-edge (a) k^3-weight EXAFS oscillations and (b) Fourier transformed (k = 3–12 Å^{-1}) of Fe foil, Fe_3C, and **Fe_{60}/C**, recorded in transmission mode.

Table S1. Summary of the magnetic data.

Sample	d [nm]	Fe loading [c] [*w*t%]	m [d] [μ_B atom$_{Fe}^{-1}$]	H_c [e] (1.9 K) [Oe]	H_c (300 K) [Oe]	T_B [f] [K]	T_C [g] [K]
Fe_3C	39 [a]	–	1.5	166	21	467	483
Fe_{60}/C	1.3±0.3 [b]	0.20	2.3	603	140	ca. 385	483±5
Fe_{28}/C	1.0±0.3 [b]	0.13	1.5	939	163	473	483±5
Fe_{12}/C	0.9±0.2 [b]	0.056	1.6	1856	367	410–470 [h]	ca. 488
Fe_4/C	–	0.013	1.0	2697	666	350–470 [h]	ca. 488

[a] Crystal diameter estimated based on PXRD data. [b] Particle diameter estimated based on TEM data. [c] Loading amount of Fe in the sample after CHR as measured using ICP-AES; the experimental error was estimated to be ca. 10%. [d] Magnetic moment per Fe atom estimated based on the saturation magnetization at 1.9 K. [e] Coercivity. [f] Blocking temperature. [g] Curie temperature. T_B and T_C were calibrated using T_C = 483 K (Fe_3C as a standard),[9] and were determined from the maximum of the second derivative of the *M*–*T* curve. [h] Uncertainty is due to the measurement sensitivity limit and noise.

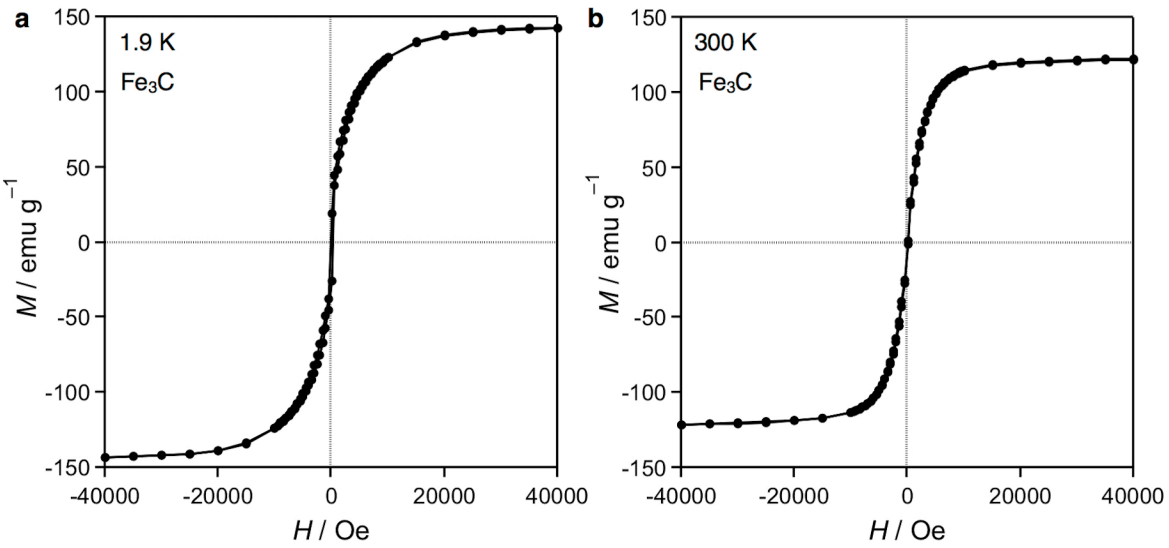

Fig. S8 The magnetization–field (*M*–*H*) loop for Fe_3C at (a) 1.9 K and (b) 300 K, for magnetization (*M*) per the sample weight.

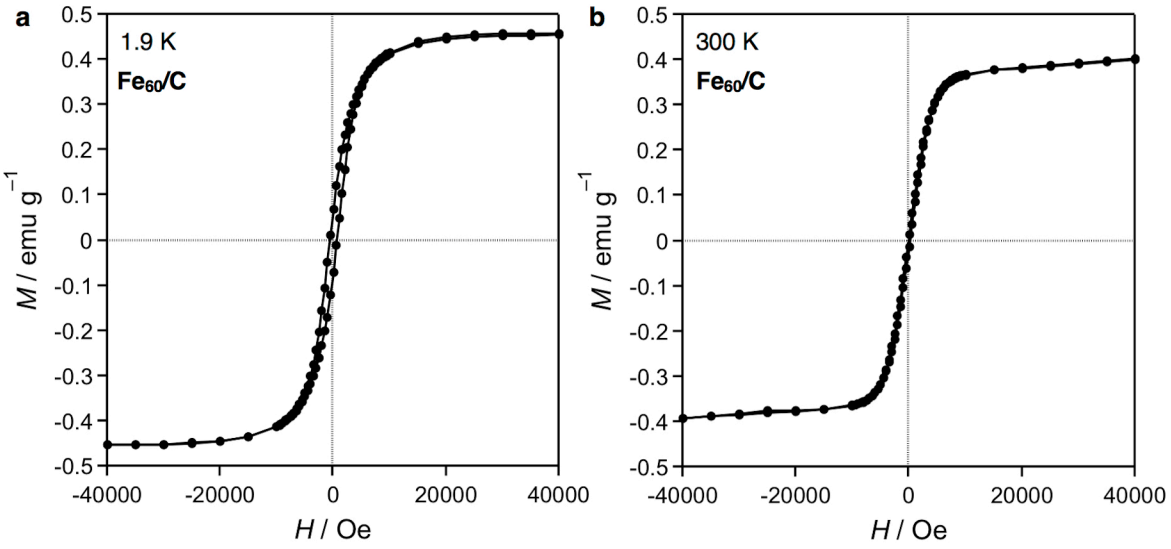

Fig. S9 The magnetization–field (*M*–*H*) loop for **Fe_{60}/C** at (a) 1.9 K and (b) 300 K, for magnetization (*M*) per the sample weight.

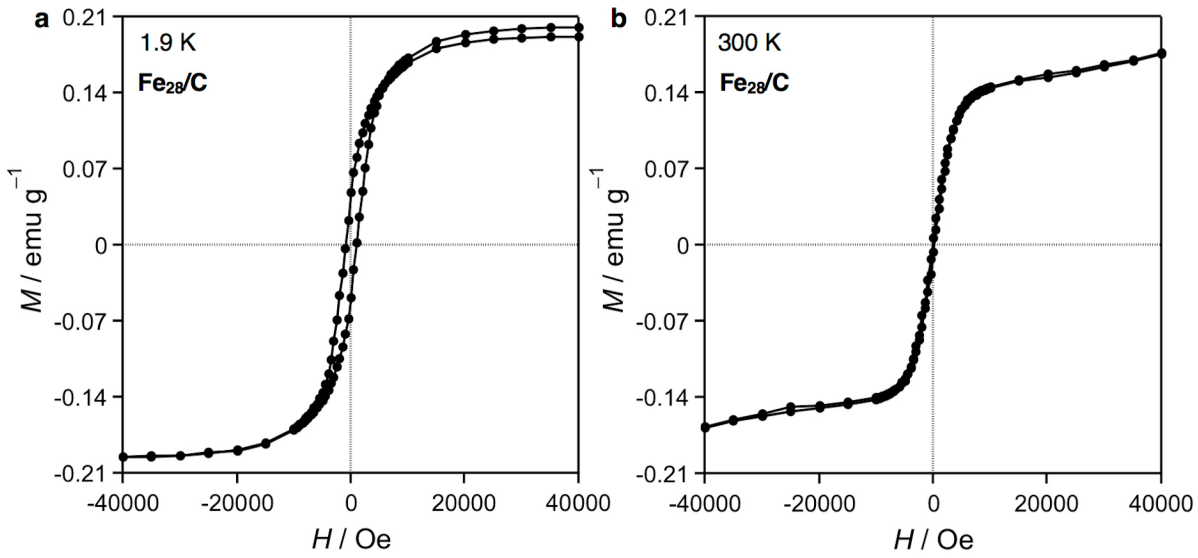

Fig. S10 The magnetization–field (*M*–*H*) loop for **Fe_{28}/C** at (a) 1.9 K and (b) 300 K, for magnetization (*M*) per the sample weight.

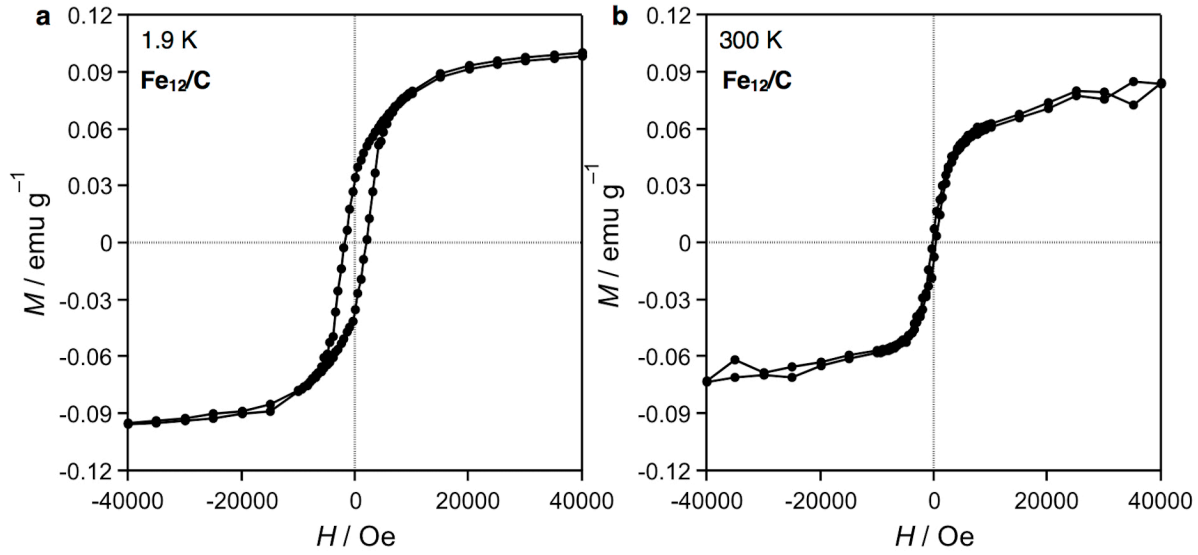

Fig. S11 The magnetization–field (*M*–*H*) loop for **Fe_{12}/C** at (a) 1.9 K and (b) 300 K, for magnetization (*M*) per the sample weight.

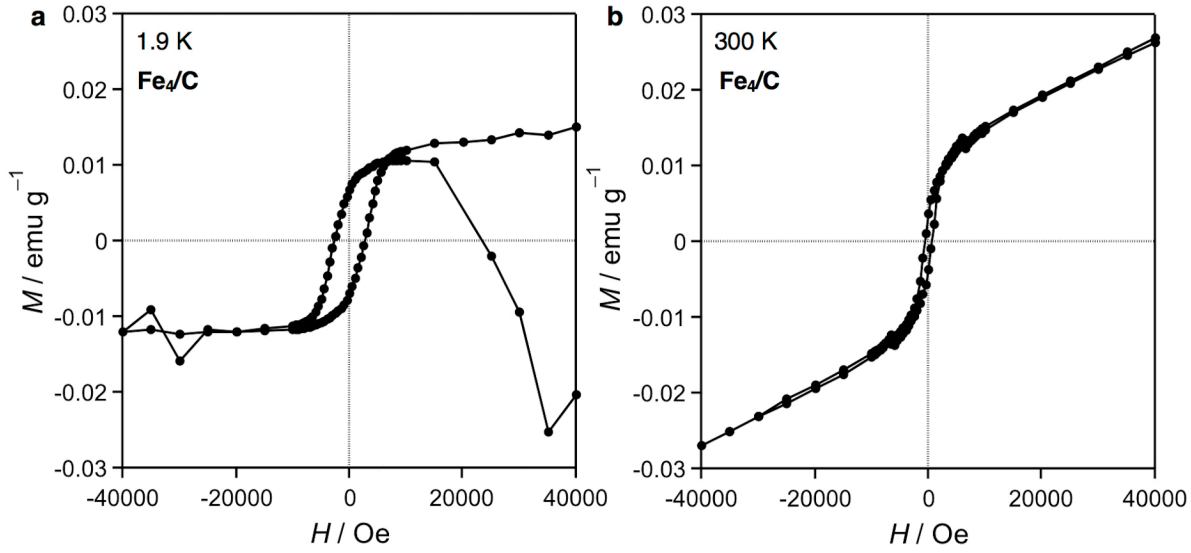

Fig. S12 The magnetization–field (*M*–*H*) loop for **Fe$_4$/C** at (a) 1.9 K and (b) 300 K, for magnetization (*M*) per the sample weight.

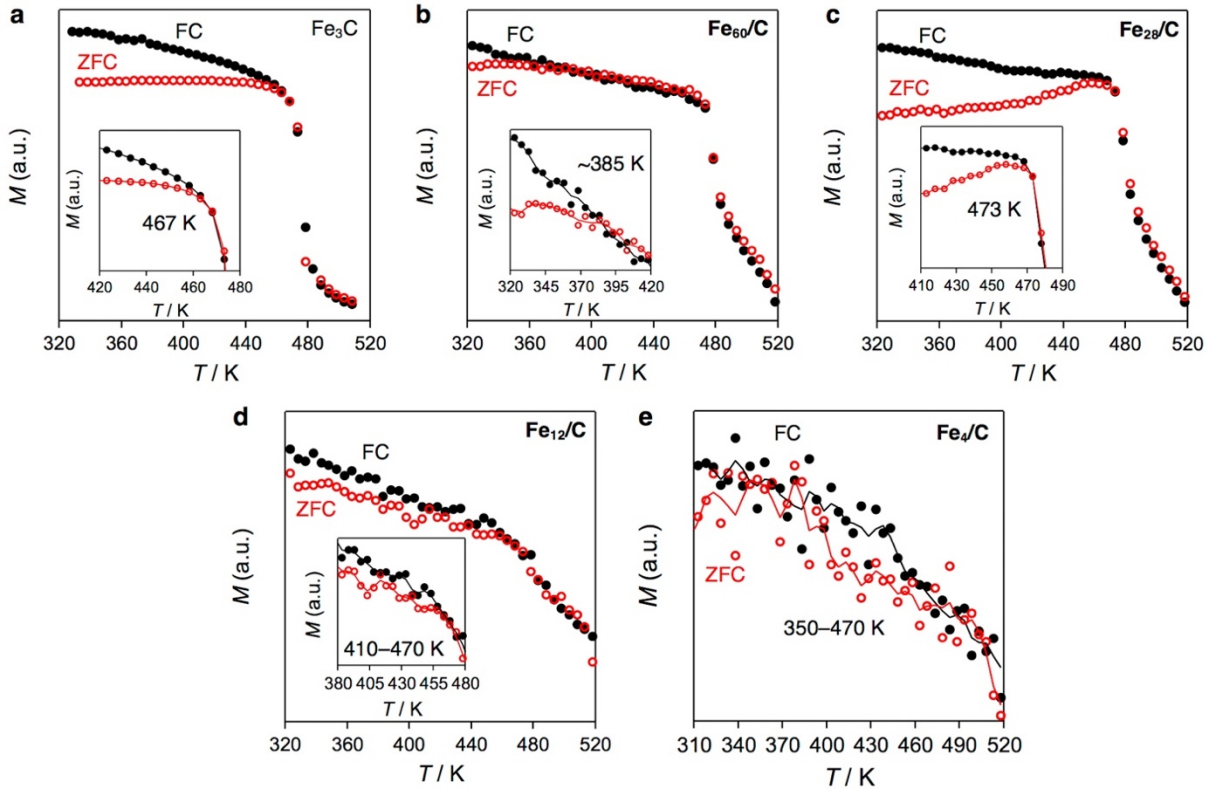

Fig. S13 Field-cooling (FC; black circles) and zero-field-cooling (ZFC; red hollow circles) magnetization curves for (a) Fe_3C, (b) **Fe$_{60}$/C**, (c) **Fe$_{28}$/C**, (d) **Fe$_{12}$/C**, and (e) **Fe$_4$/C** measured in increments of 5 K at 500 Oe. The insets show magnifications of the region near the intersection of the FC and ZFC curves, together with smoothed trend lines. The blocking temperature (T_B) was determined as the branch point of the FC and ZFC curves.

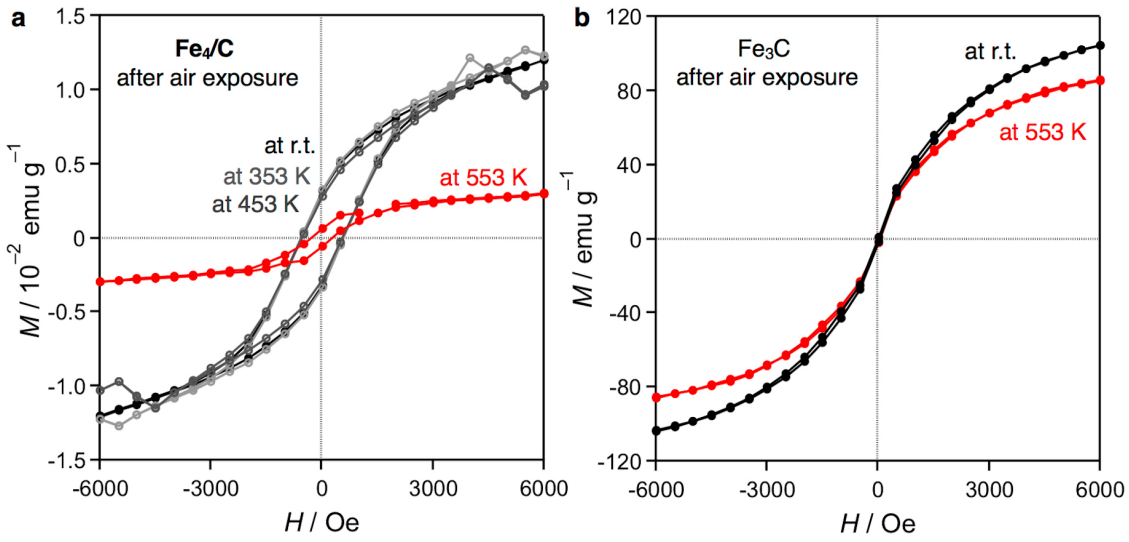

Fig. S14 The magnetization–field (*M*–*H*) loop at 300 K after air exposure for 30 min for (a) **Fe$_4$/C** (sample B) at r.t., 353, 453, and 553 K, and for (b) Fe$_3$C at r.t. and 553 K.

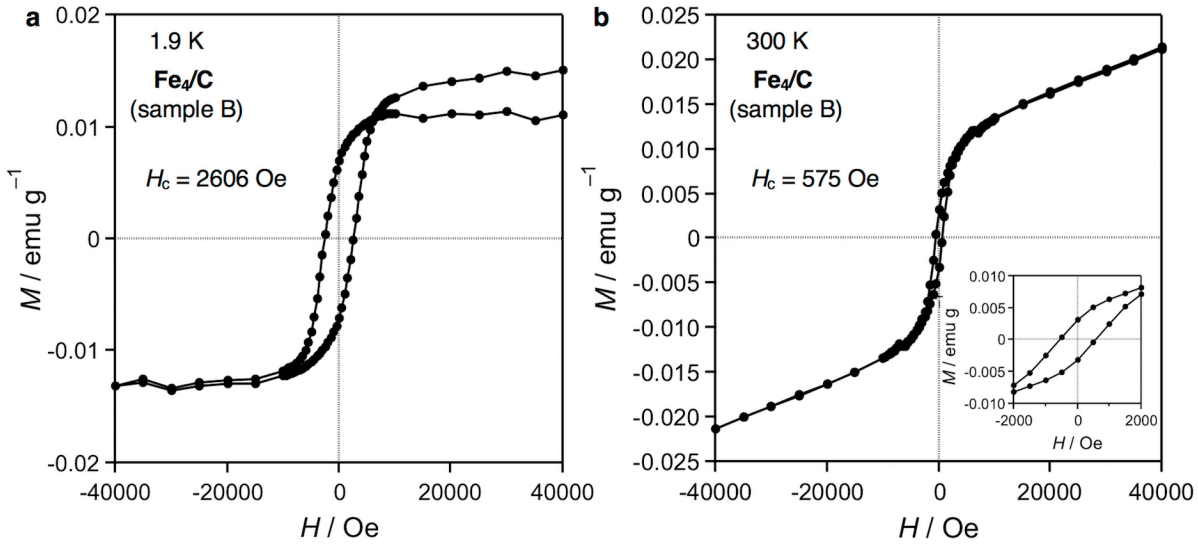

Fig. S15 The magnetization–field (*M*–*H*) loop for **Fe$_4$/C** (sample B) at (a) 1.9 K and (b) 300 K, for magnetization (*M*) per the sample weight. A reproducibility for a hysteresis *M*-*H* loop is confirmed.

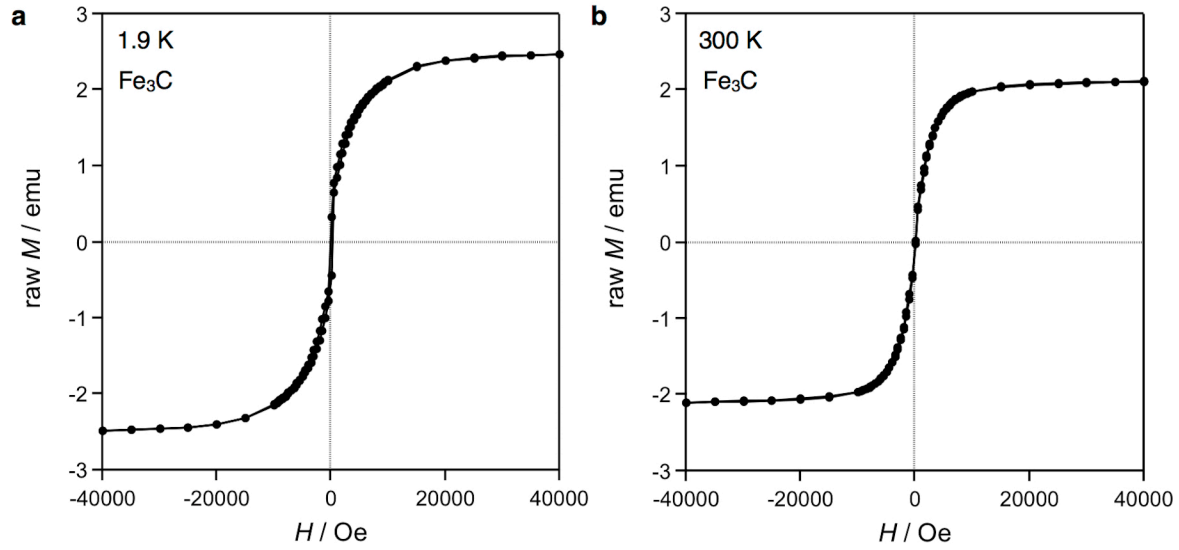

Fig. S16 The magnetization–field (*M*–*H*) loop for Fe_3C at (a) 1.9 K and (b) 300 K, for magnetization (*M*) of raw data.

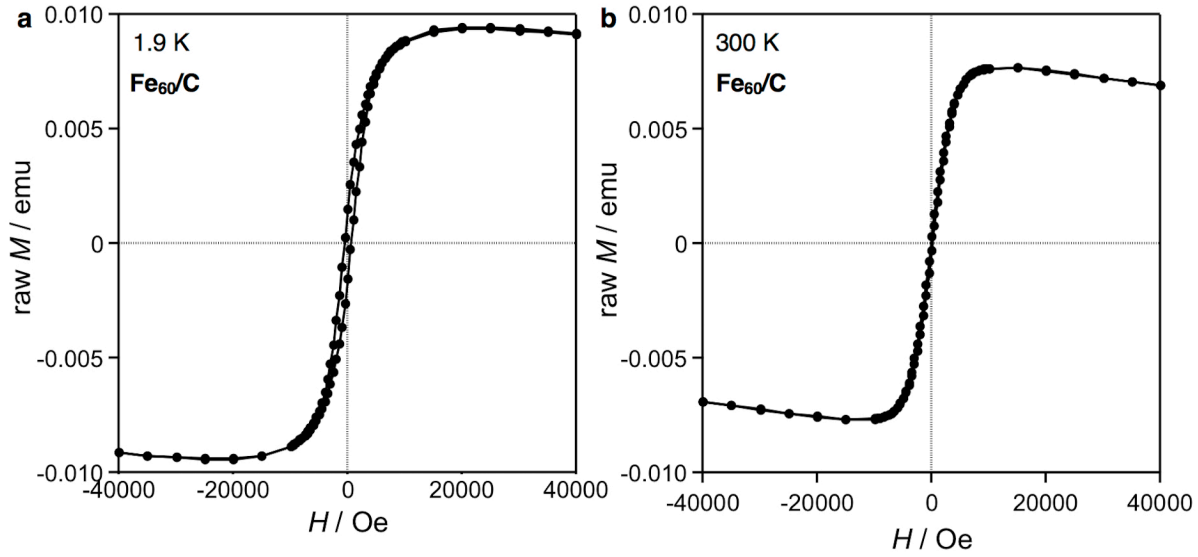

Fig. S17 The magnetization–field (*M*–*H*) loop for **Fe_{60}/C** at (a) 1.9 K and (b) 300 K, for magnetization (*M*) of raw data.

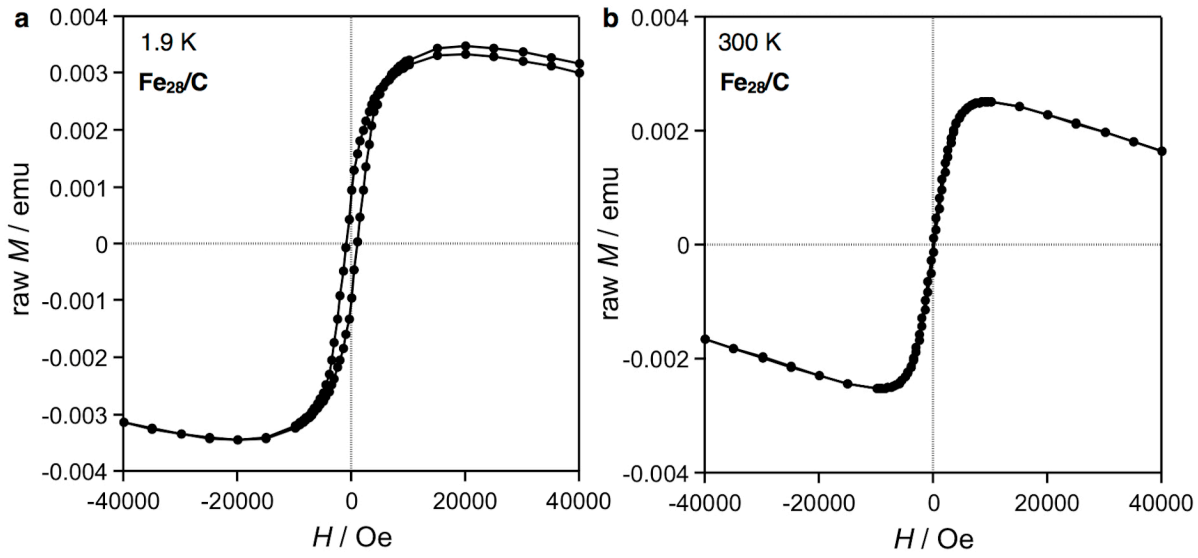

Fig. S18 The magnetization–field (*M*–*H*) loop for **Fe_{28}/C** at (a) 1.9 K and (b) 300 K, for magnetization (*M*) of raw data.

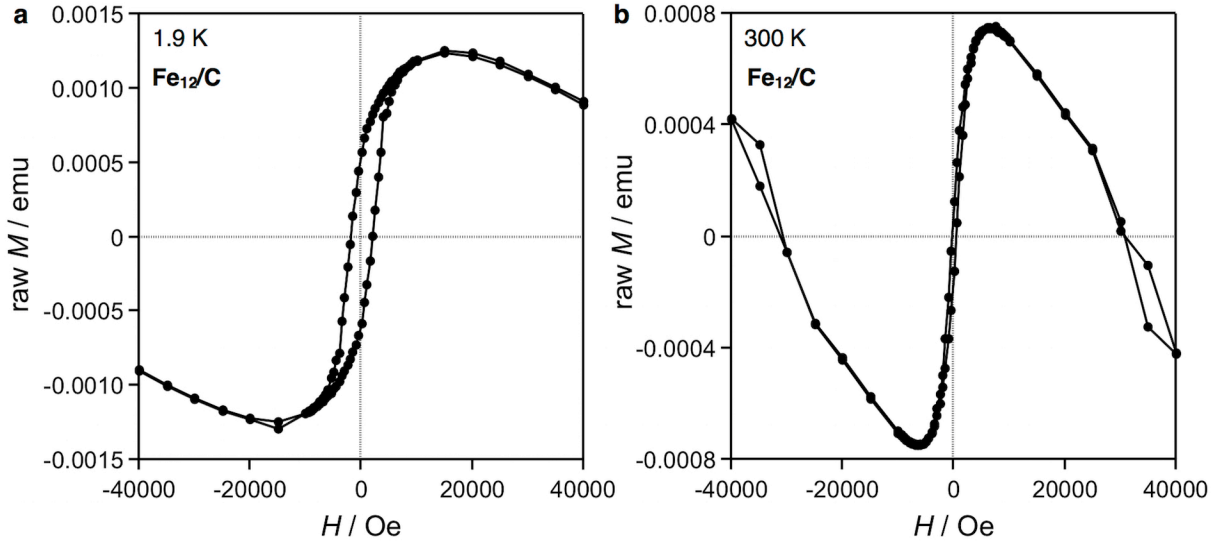

Fig. S19 The magnetization–field (*M*–*H*) loop for **Fe_{12}/C** at (a) 1.9 K and (b) 300 K, for magnetization (*M*) of raw data.

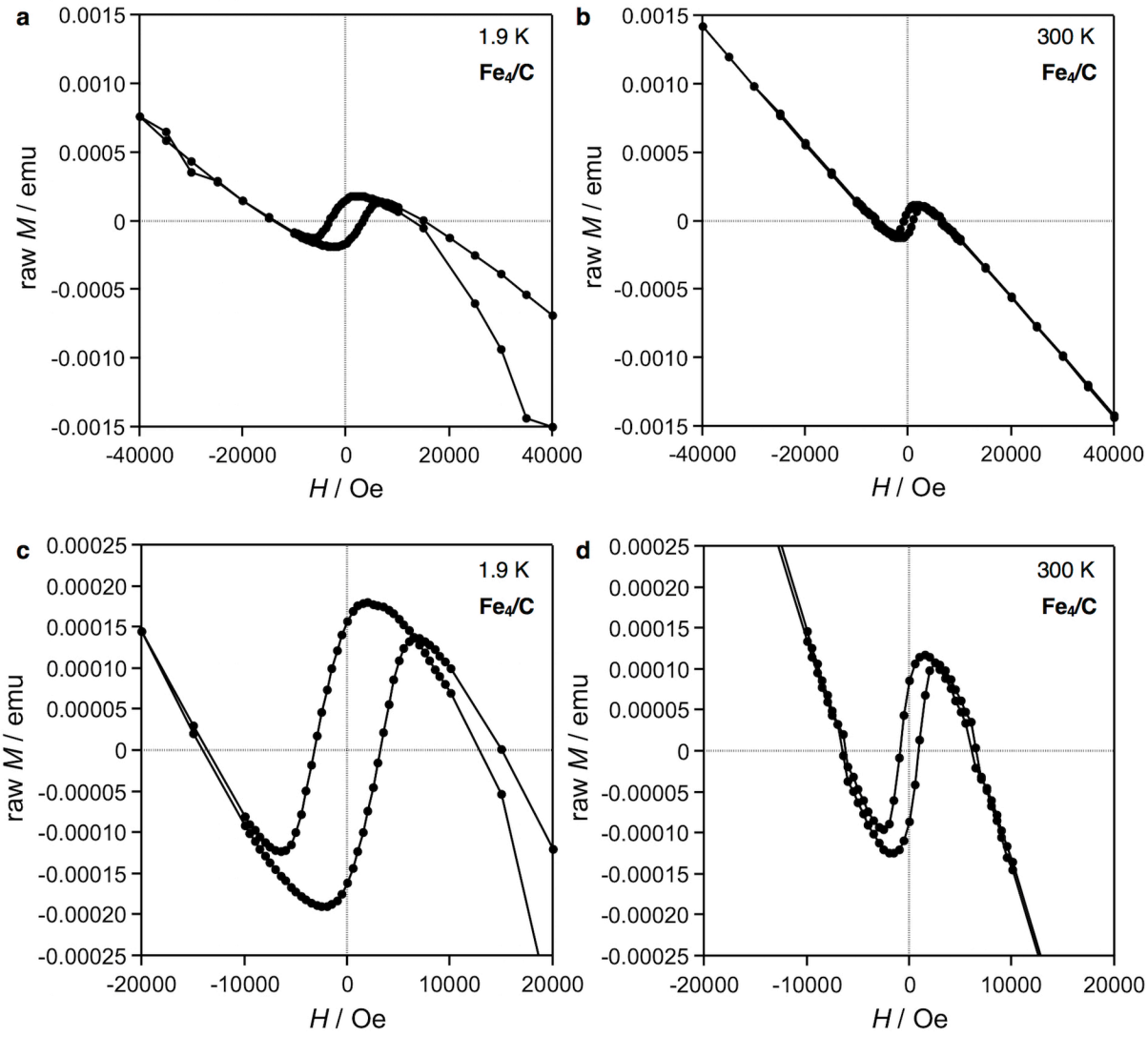

Fig. S20 The magnetization–field (*M*–*H*) loop for **Fe$_4$/C** at (a) 1.9 K and (b) 300 K, for magnetization (*M*) of raw data. (c) and (d) show magnifications around zero-field, respectively.

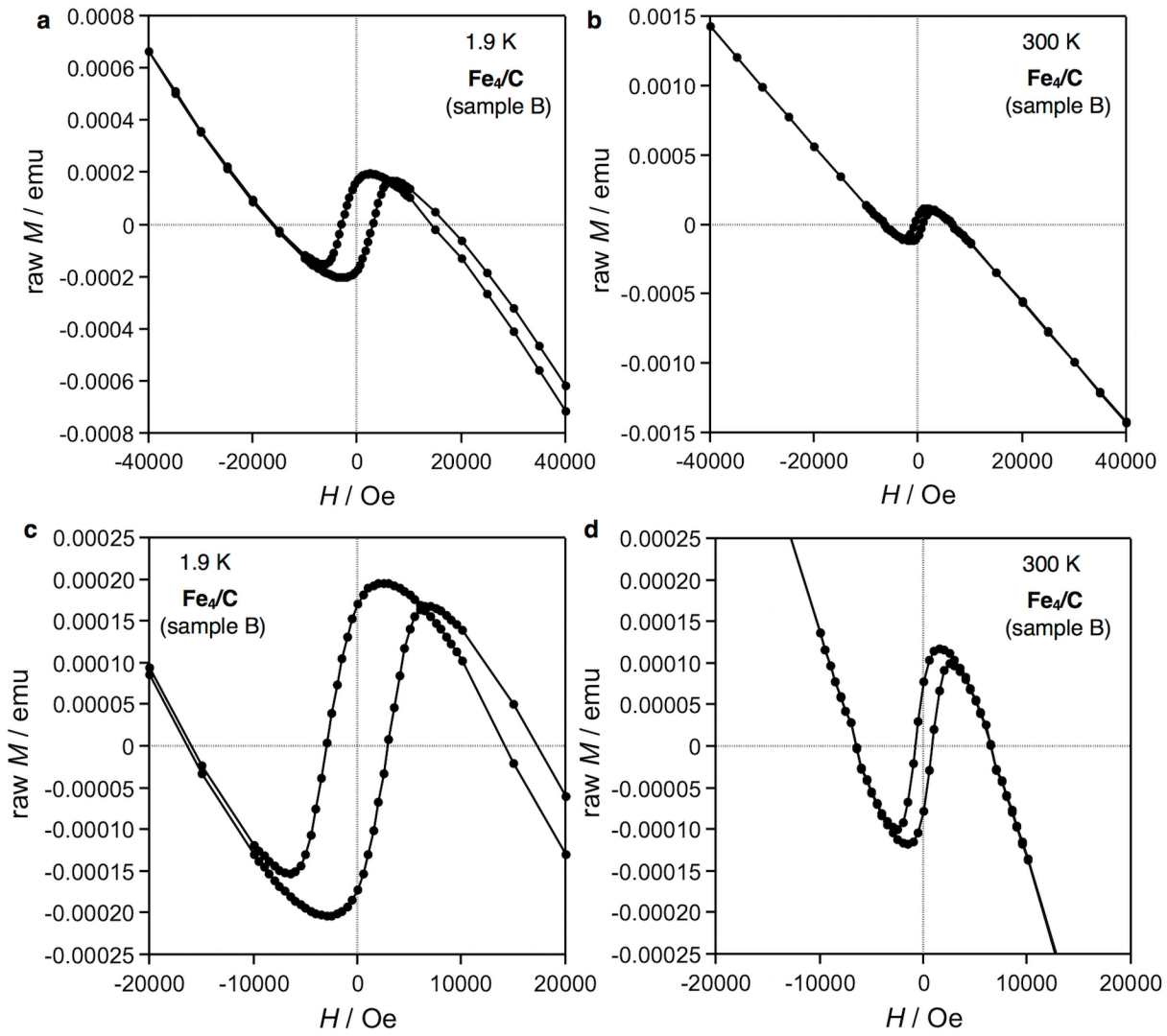

Fig. S21 The magnetization–field (*M*–*H*) loop for **Fe$_4$/C** (sample B) at (a) 1.9 K and (b) 300 K, for magnetization (*M*) of raw data. (c) and (d) show magnifications around zero-field, respectively.

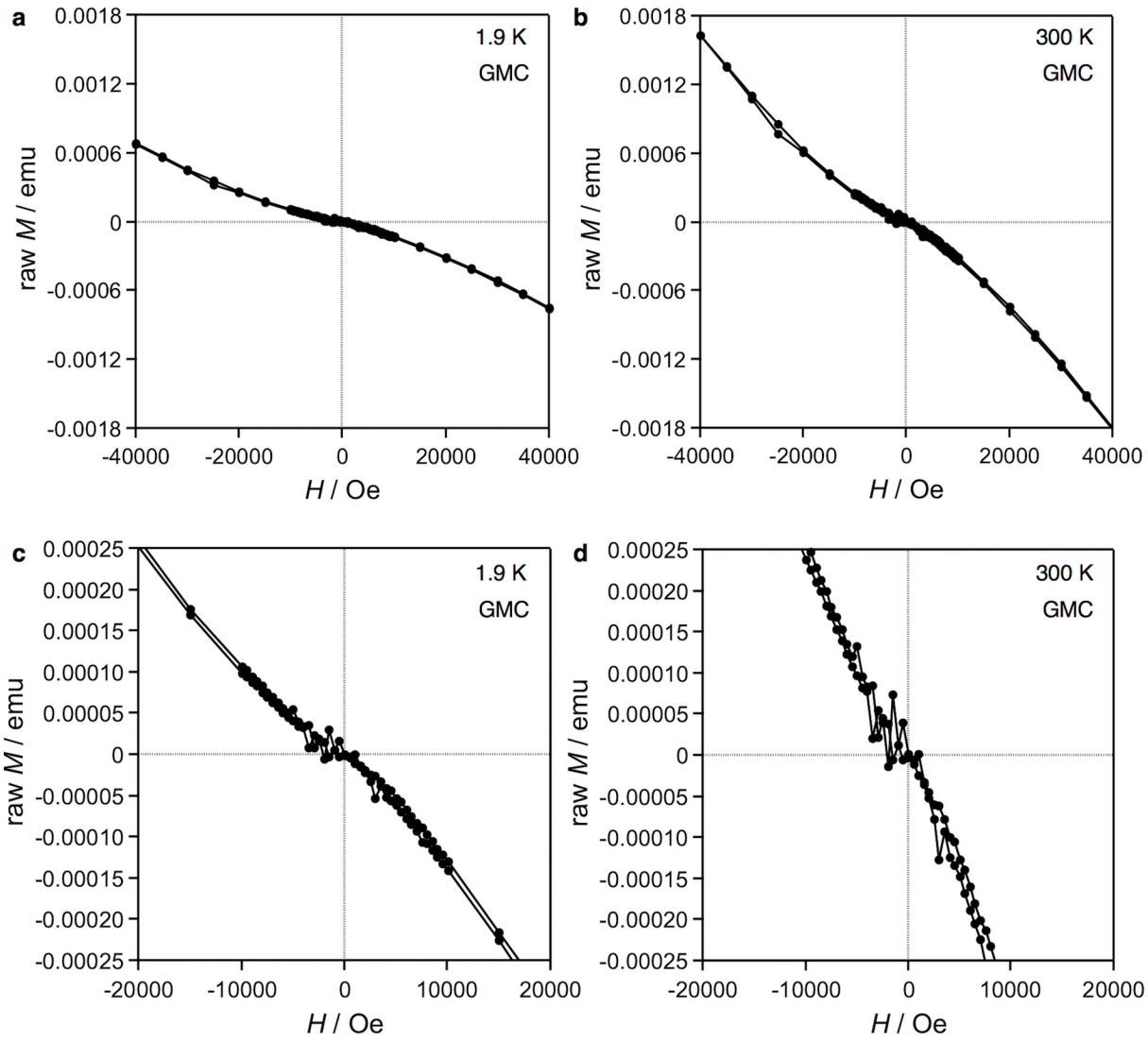

Fig. S22 The magnetization–field (*M*–*H*) loop for GMC at (a) 1.9 K and (b) 300 K, for magnetization (*M*) of raw data using a standard transport. (c) and (d) show magnifications around zero-field, respectively.

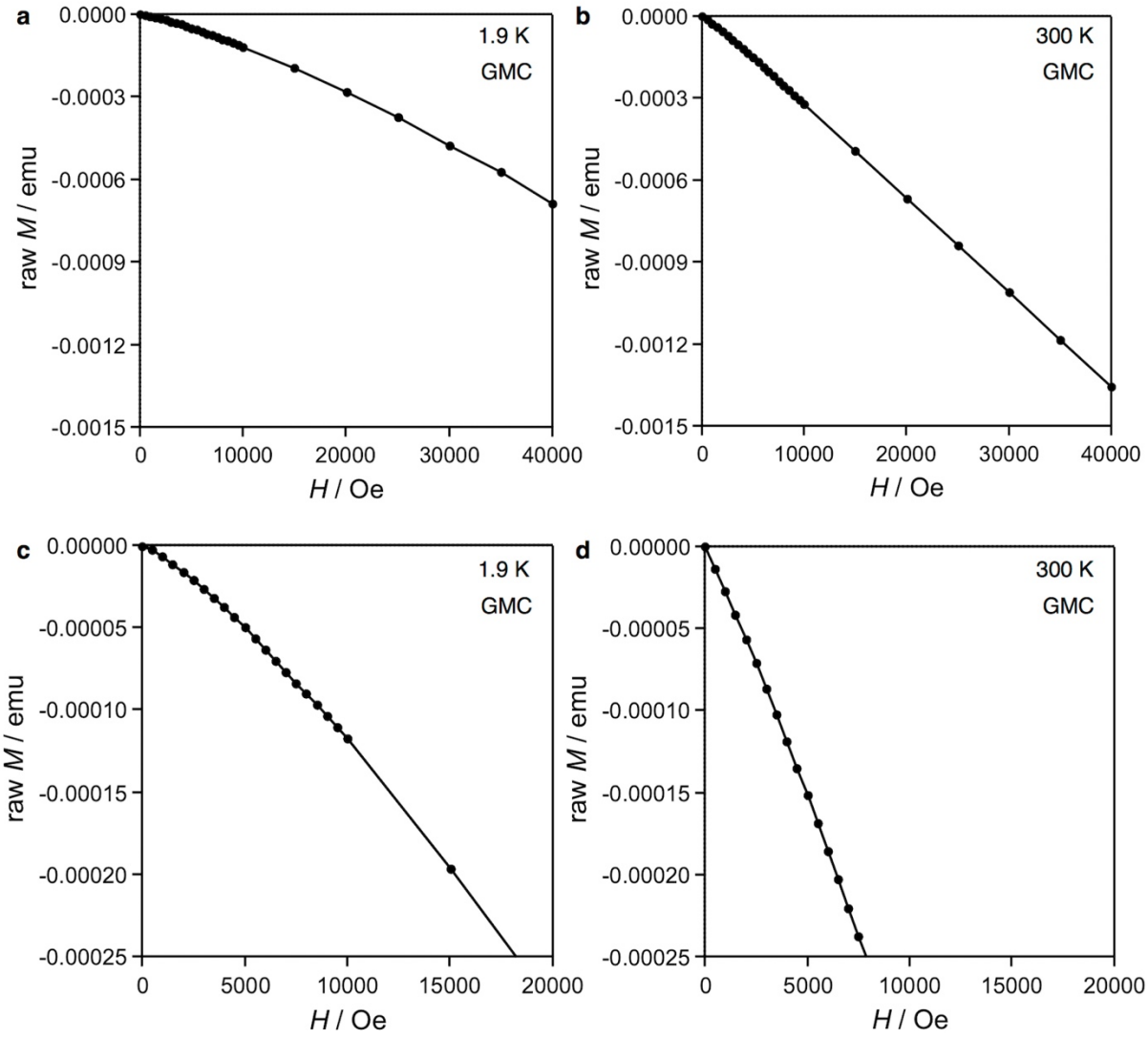

Fig. S23 The magnetization–field (*M*–*H*) loop for GMC at (a) 1.9 K and (b) 300 K, for magnetization (*M*) of raw data using a RSO transport. (c) and (d) show magnifications around zero-field, respectively.